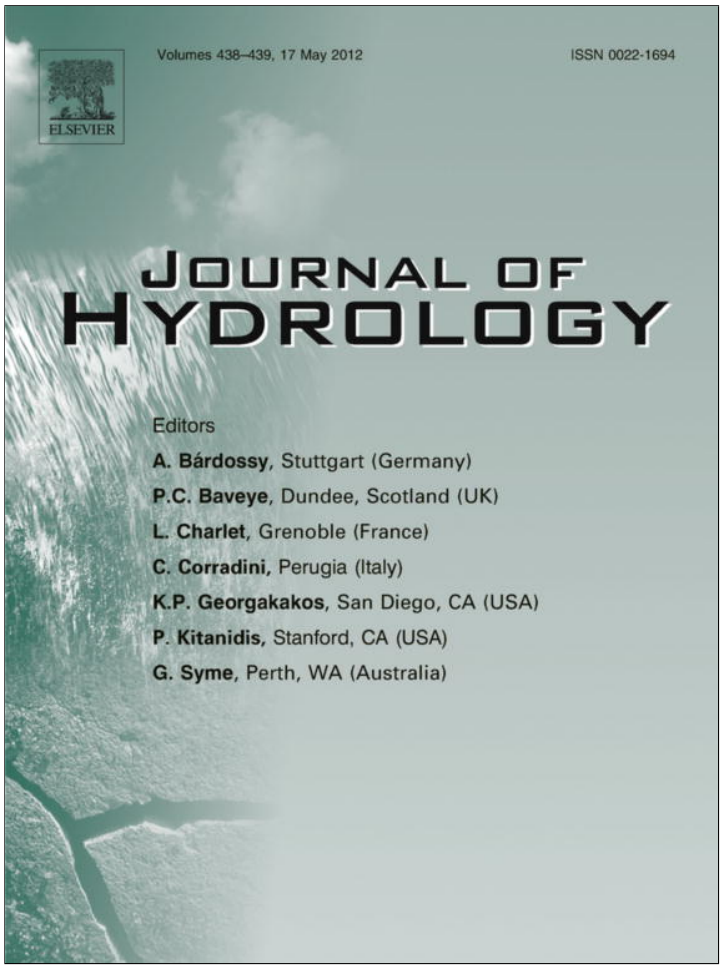

Journal of Hydrology 438–439 (2012) 203–214

Contents lists available at SciVerse ScienceDirect

Journal of Hydrology

journal homepage: www.elsevier.com/locate/jhydrol

Spatial and temporal dynamics of water flow and solute transport in a heterogeneous glacial till: The application of high-resolution profiles of $\delta^{18}O$ and $\delta^{2}H$ in pore waters

Christine Stumpp [a,b,*], M. Jim Hendry [a]

[a] Department of Geological Sciences, University of Saskatchewan, Saskatoon, SK, Canada S7N 5E2
[b] Helmholtz Zentrum München, German Research Center for Environmental Health, Institute of Groundwater Ecology, Ingolstädter Landstr. 1, D-85764 Neuherberg, Germany

ARTICLE INFO

Article history:
Received 6 December 2010
Received in revised form 28 October 2011
Accepted 14 March 2012
Available online 21 March 2012
This manuscript was handled by Philippe Baveye, Editor-in-Chief, with the assistance of Chunmiao Zheng, Associate Editor

Keywords:
Glacial till
Aquitard
Stable isotopes of water
Heterogeneity
Water flow
Solute transport

SUMMARY

The heterogeneity and dynamic of water flow and solute transport processes were investigated in the upper 6 m of a surficial, glacial till in southern Saskatchewan, Canada. Continuous core samples from three vertical sites located over a maximum spatial distance of 65 m were collected and analyzed for particle size distribution, porosity, and water content. High-resolution (0.2 m) profiles of $\delta^{18}O$ and $\delta^{2}H$ in pore waters were also measured for the three sites on a seasonal basis. Depth profiles of all measured parameters indicate highly heterogeneous structures in the upper 6 m. In two coreholes, depleted water isotopes measured at different depths below ground (0.7 and 3 m) were in the range of winter precipitation values, suggesting preferential flow of meltwater in spring accompanied by a rising water table. A one-dimensional equilibrium flow and transport model failed to simulate the isotope-depth distributions with depleted winter values, and could not reproduce the measured values even when accounting for vertical, preferential flow. A conceptual model was created, based on the consistency of all measured data and assuming preferential lateral flow as the controlling flow and transport mechanism after snowmelt. In the model, water from surface runoff (after snowmelt) drains into an ephemeral depression that crosses the study site. As this water infiltrates, it forms a water table mound that slowly propagates away from the depression. As the water table propagates outwards, dynamic vertical flow processes result in net upward and downward fluxes.

1. Introduction

Clay-rich glacial tills cover large areas of North America and Europe. They are generally considered to protect underlying aquifers from contaminants applied on or stored near ground surface (McCombie, 1997) because the hydraulic conductivity (K) of such clay-rich sediments can be low (in the range of 10^{-10} m s^{-1}) (Freeze and Cherry, 1979; Keller et al., 1988; Shaw and Hendry, 1998). Despite their importance, little is known about the heterogeneity of solute transport in such systems. In non-fractured tills, transport is dominated by diffusion (Harrington and Hendry, 2005). However, this may not be the case in fractured tills, which commonly blanket the upper surface (Harrar et al., 2007; Joergensen et al., 2004; Shaw and Hendry, 1998). The presence of fracturing can result in the bulk K of the till being one to three orders of magnitude greater than the matrix K. Under these conditions, water and solutes can migrate great distances via advection (Cuthbert et al., 2010; D'Astous et al., 1989; Helmke et al., 2005; Joergensen and Fredericia, 1992; Joergensen et al., 2004; McKay and Fredericia, 1995; McKay et al., 1999). Similarly, laterally extensive sand streaks and layers can also provide avenues through which water and solutes can advect (Hendry and Wassenaar, 2009; Joergensen et al., 2004; McKay and Fredericia, 1995). Due to low infiltration capacities in clay-rich tills, surface runoff may be an important component in the water balance, particularly in undulating landscapes formed after glaciation. Surface runoff and ponding in topographic depressions can play a crucial role in spatial and temporal recharge patterns (Gerke et al., 2010; Hayashi et al., 2003) or even form a groundwater dependent ecosystem (van der Kamp and Hayashi, 2009).

To define the influence of fractures, water flow and solute transport parameters have been determined in tills using single, artificial tracer injections (Gerke and Köhne, 2004; Harrar et al., 2007; Mortensen et al., 2004; Rosenbom et al., 2008). Such investigations are of value for saturated conditions and short mean transit times. For studies in unsaturated media, single tracer injections cannot be

* Corresponding author at: Helmholtz Zentrum München, German Research Center for Environmental Health, Institute of Groundwater Ecology, Ingolstädter Landstr. 1, D-85764 Neuherberg, Germany. Tel.: +49 89 3187 4165; fax: +49 89 3187 3361.
E-mail address: christine.stumpp@helmholtz-muenchen.de (C. Stumpp).

0022-1694/$ - see front matter © 2012 Elsevier B.V. All rights reserved.
http://dx.doi.org/10.1016/j.jhydrol.2012.03.024

employed to study the variable initial and boundary conditions that occur under field conditions. However, naturally occurring stable isotopes of water ($\delta^{18}O$ and $\delta^{2}H$) can provide information about spatial and temporal heterogeneities with respect to transient flow and transport processes in both saturated and unsaturated porous or fractured media (Darling and Bath, 1988; Hendry and Wassenaar, 1999, 2009; Joshi and Maulé, 2000; Keller et al., 1988; Stumpp et al., 2009a,b). Stable isotopes of water can also aid in understanding the importance of processes such as evaporation (Barnes and Allison, 1988; DePaolo et al., 2004) or preferential flow (Stumpp et al., 2007). In addition, isotope transport modelling can provide quantitative interpretations of flow processes from depth profiles, even assuming simplified steady state and homogeneous conditions (Singleton et al., 2004).

To date, most studies have focused on saturated, non-fractured till or unsaturated, fractured soils covering the till. To improve upon our understanding of water and solute migration between ground surface and the depth at which diffusion-controlled transport occurs in till, this study examines the spatial and temporal dynamics in water flow and solute transport processes in an oxidized and underlying unoxidized zone of a glacial till and develops a conceptual model to describe heterogeneous and dynamic water flow and transport in landscapes formed by sediments with low infiltration capacities. The study investigates dynamic flow and transport regions as well as diffusion-dominated regions, and, specifically, whether these regions are limited to the oxidized and unoxidized till zones and how they are related to the water table.

The objectives were achieved by measuring water levels in piezometers and a water table well installed in the oxidized and unoxidized zones as well as characterizing the till sediments. Further, high-resolution profiles of $\delta^{18}O$ and $\delta^{2}H$ in pore waters were measured using a new laser technology. For the first time, samples were collected seasonally with high vertical resolution from the surface to 6 m below ground (BG), including the soil, the vadose zone, and the saturated zone, at three sites. One-dimensional numerical modelling of the migration of water and the isotopes of water was performed using an equilibrium water flow and solute transport model. Based on the available data, a conceptual model that describes dynamic vertical and lateral water flow as well as solute transport and heterogeneities was created.

2. Materials and methods

2.1. Study site

The study was conducted at a long-term glacial till research site located in southern Saskatchewan, about 140 km south of Saskatoon, Canada (the King Site; 51°05′N, 106°5′W). The geology at the site consists of 80 m of plastic clay-rich Battleford till. The surficial 3–5 m of till is oxidized (brown color) and visibly fractured (Hendry and Wassenaar, 2009; Shaw and Hendry, 1998). The underlying till is massive, unoxidized (dark gray color), and non-fractured. Bulk K values in the oxidized till (10^{-8}–10^{-9} m s^{-1}) are two orders of magnitude greater than in the unoxidized till (10^{-10}–10^{-11} m s^{-1}), with the difference attributed to the presence of fractures (Shaw and Hendry, 1998). The soils of the area (Weyburn association) developed on the glacial till and are commonly Dark Brown Chernozems (Ellis et al., 1970). Although the overall topography is flat (±0.8 m), the micro-topography (Fig. 1) is characterized by subtle topographic features (±0.4 m). A 0.4–0.6 m deep and 3–6 m wide drainage ditch, located along a natural swale, runs W–E through the northern half of the site (Fig. 1) and is used to remove spring meltwater from the area.

The semi-arid continental climate of this region is characterized by long, cold winters and short, warm summers. Precipitation and climatic data (1999–2008; Environment Canada, unpublished data) were compiled for the town of Beechy, 40 km southeast of the site. Daily climatic data were used to determine potential evapotranspiration (ETp) with the Hargreaves method, resulting in mean annual ETp of 838 ± 43 mm, which considerably exceeds the mean annual precipitation (336 ± 82 mm). About 75% of the precipitation falls between May and September, coincident with the greatest determined ETp (82–168 mm month^{-1}). Winter precipitation falls mostly as snow. The mean annual air temperature was 4 °C.

2.2. Sampling and analyses

2.2.1. Hydraulic measurements

Twenty-two piezometers were installed at various depths within the till between September and December 1995, as described in detail by Shaw and Hendry (1998). Nine of these piezometers (with 1.5 m long intake zones) completed between 2 and 12.4 m BG were used in this study (Fig. 1). Since construction, water levels have been measured manually and regularly (about once a month) in all piezometers as well as in a water table well (WTW, installed to 3.2 BG) (Fig. 1).

2.2.2. Core sampling

In December 2007, continuous sediment cores were collected at BV1 and BV2 (Fig. 1, referred to as I) using a split spoon sampler (1.52 m long × 0.07 m diameter) to 15 and 18 m BG. $\delta^{2}H$ and $\delta^{18}O$ were measured for subsamples of these cores at a resolution of 0.3 m. These high-resolution vertical profiles, reported in Hendry and Wassenaar (2009), were used as initial investigations for the current study. Between June and September 2009, continuous core samples were collected at BV1, BV2, and an additional site on three occasions (II: 02.06.09, III: 31.07.09, IV: 28.09.09) using the same technique as Hendry and Wassenaar (2009) but to 6 m BG. The third site (BG32; Fig. 1) was selected for study because it contained elevated salt concentrations (Harrington and Hendry, 2005) that suggested site-specific solute transport mechanisms. In addition, grab samples were collected at the three sites to 1–1.5 m BG using a hand auger during the July and September sampling dates. All core samples for the sampling times (I–IV) were collected within 1 m radial distance from the original core sites in a clockwise direction (Fig. 1). Core holes were sealed with bentonite after drilling.

The distances between sites BV1 and BV2, BV1 and BG32, and BV2 and BG32 were 63, 56, and 19 m, respectively. The distances between sites BV1, BV2, BG32, and the WTW were 56, 14, and 5 m, respectively. The distances from the sites to the various piezometers ranged from 0 to 70 m (Fig. 1).

After visual observations (e.g., colors, presence of salt crystals, the transition between oxidized and unoxidized zones) in the field, cores were immediately cut into 0.1 m long sub-samples and sealed in double Ziploc® bags to minimize vapor loss prior to analyses, in the manner described by Hendry and Wassenaar (2009). Alternate core samples were used to measure water isotopes ($\delta^{2}H$ and $\delta^{18}O$) and sediment properties (water content, porosity, and bulk density), providing a core depth resolution of 0.2 m for both data sets for all sampling dates in 2009. The hand auger samples were collected with a depth resolution of 0.1 m and were only analyzed for water isotopes.

Soil horizons and structure were identified for the upper 0.5 m BG across the site during the June 2009 sampling campaign. Due to uniform soil development, a location not influenced by any drilling activities at the research site was chosen for detailed sampling (10 m northeast of BV1; Fig. 1). Bulk material was collected from each horizon for textural analysis. Further, three volumetric samples (10^{-4} m^{3}) were collected from each soil horizon in stainless

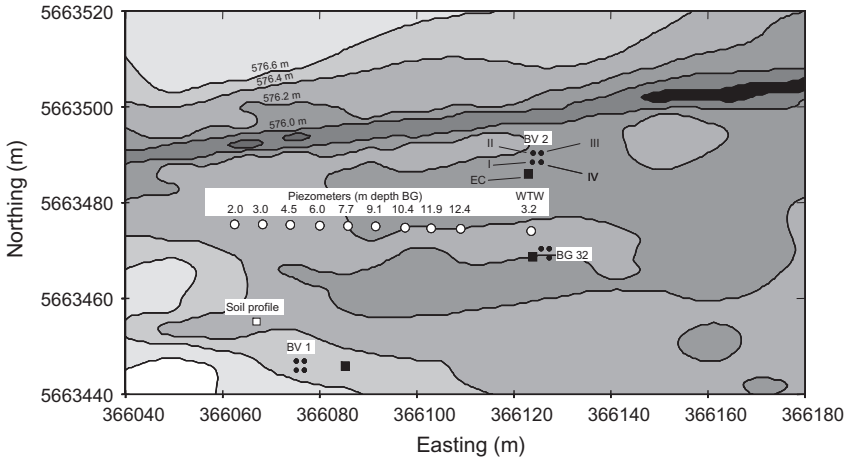

Fig. 1. Micro-topography of the King Site (after Harrington and Hendry, 2005) and the location of piezometers, water table well (WTW), soil profile test site, the core holes (black circles), and the electric conductivity measurements (black squares). Contour lines reflect topography at 0.2 m intervals with darker shaded zones being lower in elevation than the lighter zones. Core holes at the three locations (BV1, BV2, BG32) were collected clockwise at the different sampling times (I–IV) at a distance of 1 m.

steel cylinders during the June sampling campaign and used to determine the water retention characteristics of the media.

2.2.3. Analyses of sediment properties

Particle sizes were determined for samples collected during the June 2009 sampling campaign from the soil horizons, in cores collected at regular depth intervals, and at textural breaks in the cores using ASTM D-422-63 (ASTM, 2007). Particle sizes (<4.75 mm) were determined using the hydrometer method (ASTM: sand >0.075 mm, silt 0.075–0.005 mm, clay <0.005 mm). Particle density was determined using the pycnometer method (Blake, 1965b) on samples analyzed for particle size distribution.

Water contents (Gardner, 1965), porosities (Vomocil, 1965), and bulk densities (Blake, 1965a) were analyzed on all cores collected in 2009 (with a vertical resolution of 0.2 m). Representative volume specific sub-samples were collected from these cores using a cylinder ($\sim 35 \times 10^{-6}$ m^3) for which the total wet and dry mass were determined. The sub-samples and the remainder of the cores were dried at 105 °C for 48 h to determine bulk densities (kg dry mass/m^3 volume) as well as gravimetric (kg water/kg dry mass) and volumetric (m^3 water/m^3 volume) water contents. Once the samples were dry, color was determined using a Munsell soil color chart; the presence of any salt crystal development after drying was noted.

Water contents and suctions were determined on samples from each soil horizon in triplicate and on core samples from four depths (approx. 0.6, 1.7, 2.5, and 3.9 m) within volume specific sub-samples ($\sim 35 \times 10^{-6}$ m^3) from the three sites during the July 2009 sampling campaign. Water-retention characteristics were determined using a 5 and 15 bar pressure plate extractor (Soilmoisture Equipment Corp, Santa Barbara) (Richards, 1965). Saturated hydraulic conductivities (K_s) were measured twice near the surface (B- and C-horizon) within 2 m from each site with a Guelph permeameter (Soilmoisture Equipment Corp., 1986).

2.2.4. Stable isotopes of water

The δ^2H and δ^{18}O in the sub-samples were measured using $H_2O_{(liquid)}$–$H_2O_{(vapor)}$ pore water equilibration and off-axis laser spectroscopy (Wassenaar et al., 2008). Equilibrium between the water in the sediment cores and the gas phase was reached after three days of exposure to dry air. The water vapor was continuously sampled in the headspace using a water vapor analyzer (LGR model 908-004; www.lgrinc.com). This method allows both δ^2H and δ^{18}O to be measured directly on soil cores with volumetric water contents >5%, with an accuracy of $\leqslant$2‰ and $\leqslant$0.4‰ for δ^2H and δ^{18}O, respectively (Wassenaar et al., 2008).

2.3. Modelling

An equilibrium water flow and solute transport model was used to obtain insights into vertical water flow and isotope transport mechanisms in the till. Water flow was calculated using the Richards equation:

$$\frac{\partial\theta}{\partial t} = \frac{\partial q}{\partial z} = \frac{\partial}{\partial z}\left[K(h)\frac{\partial h}{\partial z} - K(h)\right] \quad (1)$$

where z is the depth (L), q is the water flux (L T^{-1}), t is the time, and $K(h)$ is the soil K (L T^{-1}), which is a function of the pressure head, h (L), and the volumetric water content, θ (L^3 L^{-3}). The water-retention and conductivity functions, θ(h) and K(h), are described by van Genuchten (1980) based on the Mualem approach (Mualem, 1979):

$$\theta(h) = \begin{cases} \theta_r + \frac{\theta_s - \theta_r}{\left[1+|\alpha\cdot h|^n\right]^m} & h < 0 \\ \theta_s & h \geq 0 \end{cases} \quad (2)$$

$$K_r(h) = \frac{[1-(\alpha\cdot h)^{n-1}\cdot[1+(\alpha\cdot h)^n]^{-m}]^2}{[1+(\alpha\cdot h)^n]^{\frac{m}{2}}} \quad (3)$$

where θ_s (L^3 L^{-3}) and θ_r (L^3 L^{-3}) are the saturated and residual water contents and α (L^{-1}), n(–), and m(–) are empirical parameters defining the shape of the retention curves, where $m = 1–1/n$. $K_r(h)$ is the relative K function, which is the ratio of the K function, $K(h)$, and K_s.

Assuming a single porous medium (all water is mobile), solute transport is described by the advection–dispersion equation for an ideal dissolved tracer:

$$\frac{\partial(\theta C)}{\partial t} = \frac{\partial}{\partial z}\left(\theta D\frac{\partial C}{\partial z}\right) - \frac{\partial(qC)}{\partial z} \quad (4)$$

where C is the tracer concentration and D is the hydrodynamic dispersion coefficient.

Water flow and isotope transport using the above equations were modeled with HYDRUS 1D (Simunek et al., 2005). We used a version of the solute transport modified for the use of the stable isotopes of water (Stumpp et al., 2012). Evaporation from the upper boundary for solute transport was defined as having no effect on the isotope delta values. In contrast, solutes concentrate near the upper boundary as water and isotopes of water leave the soil profile via evaporation.

3. Results and discussion

3.1. Hydrogeology

The depth of the water table was measured at the water table well located in the middle of the site (Fig. 1). The water table ranged in depth from 1 to 3 m BG (Fig. 2). These data exhibit a well-defined cyclic pattern of a rapid rise in the spring followed by a gradual decrease throughout the remainder of the year. During the 2009 study period, the depth to the water table decreased from 1.10 m (June) to 1.80 m (July) and 2.25 m (September) BG (575.3, 574.6 and 574.2 m asl, respectively). The rapid rise in the water table in the spring is attributed to infiltration of the melting winter snowpack. The cause for the gradual decrease in the water table throughout the remainder of the year (excluding responses from infrequent intense rainfall events) cannot be determined from the water table data (discussed below); however, it could be attributed to evapotranspiration (see study site above) and/or lateral groundwater migration. The pressure heads measured in the shallow piezometers (2.0–6.0 m BG) reflect the cyclical response in the water-table well (Fig. 2) and suggest a dynamic response of pressure heads across this zone. The consistency of the water-level responses between the water table and these piezometers suggest uniform water levels across the middle of the site (Fig. 1).

Vertical hydraulic gradients were calculated between the water levels measured in the piezometers (1997–2009). The mean vertical gradients yield upward and downward gradients; for example, gradients vary from 0.01 upwards (between 6.2 and 9.1 m BG) to 0.22 downwards (between 0.5 and 3 m BG). The measurements used to determine mean gradients were biased toward spring and summer values due to a lack of head measurements during the winter (inaccessibility of site during winter months) and because the water table was below the bottom of the screened interval in some shallow piezometers (<3 m BG) during autumn and winter periods. Seasonal variations in the gradients are evident at all depths, with downward gradients in spring and upward gradients in autumn and winter. Data from deeper piezometers yield mean vertical downward gradients of 0.014 (±0.012) between 18 and 64 m BG. All calculated vertical hydraulic gradients were in keeping with those determined from earlier studies at the site (Shaw and Hendry, 1998).

The measured K_s varied between 10^{-8} and 10^{-6} m s^{-1} near ground surface (0.25–0.45 m), with the greatest values at BG32 and smallest values at BV2. In two of six measurements (i.e., at BV2 and BV1), no water flow was measured. Thus, these tests yield order of magnitude estimates of K_s that decrease from about 10^{-6}–10^{-8} m s^{-1} near the soil surface to reported K values of 10^{-8}–10^{-9} m s^{-1} for the oxidized till and 10^{-10}–10^{-11} m s^{-1} for the unoxidized till (Harrington et al., 2007; Shaw and Hendry, 1998). Based on these K data and the small vertical hydraulic gradients, groundwater fluxes and velocities should be minimal. K values and porosities (which will be discussed later) are greater closer to the surface, indicating the same should be the case for water fluxes and velocities. Assuming a mean downward gradient of 0.1 for the summer months and a mean porosity of 0.4 in the oxidized till as well as an annual mean downward gradient of 0.03 and a mean porosity of 0.3 in the unoxidized till results in water velocities of 8×10^{-3} to 8×10^{-2} m a^{-1} for saturated conditions in the oxidized till and 3×10^{-5} to 3×10^{-4} m a^{-1} in the unoxidized till. The latter values are in accordance with average pore water velocities in the unoxidized till of 5×10^{-5} and 8×10^{-5} m a^{-1} reported by Shaw and Hendry (Shaw and Hendry, 1998).

3.2. Sediment characteristics

Three Chernozemic silty loam soil horizons were identified. Soil horizon thicknesses at the site were consistent between core locations: the Ah soil horizon (0–0.1 m BG) consisted of 21% sand, 70% silt, and 9% clay and contained roots (prairie grasses); the mineral B horizon (0.1–0.35 m BG) consisted of 16% sand, 77% silt, and 7% clay; and the C horizon (>0.35 m BG) consisted of 6% sand, 82% silt, and 12% clay and contained none to few visible roots. The structure throughout the three soil horizons was mainly angular to subangular polyhedral.

The spatial structural and textural properties of the till varied across the site and were not as homogeneous as previously suggested (Christiansen, 1971). On average, the profiles consisted of 32% sand, 47% silt, and 21% clay (Fig. 3a–c). The particle size distribution at BV1 is uniform with depth through most of the profile, with a sand content of about 40% at depths >1 m BG and more uniform clay and silt contents at depths >2 m BG; a higher clay content is also noted at 0.6 m BG. In contrast, more heterogeneous particle-size distributions were measured at BV2 and BG32. Both of these sites contain a silty loam layer, located between 2.5–2.7 m BG at BV2 and 2.8–3.6 m BG at BG32. Greater silt and lower sand contents are evident near ground surface at BG32 than at BV1 and BV2. At depths >3.6 m BG, all three profiles yield similar particle size distributions that reflect the parent material. Particle density is constant throughout each depth profile (mean = 2648 ± 41 kg m^{-3}), with the greatest values at BV1 (2673 ± 34 kg m^{-3}), followed by BG 32 (2656 ± 38 kg m^{-3}) and BV2 (2612 ± 29 kg m^{-3}).

Sediment color changes in BV2 and BG32 support the textural heterogeneity described above. For example, the color was uniform to 3.6 m BG (2.5Y 7/2, dry) at BV1 (no discontinuous silty loam layer). Core samples from BV2 and BG32 were lighter from 2.0–3.2 m (2.5Y 7/3, dry) and 2.0–3.6 m (2.5Y 6/3, dry) compared

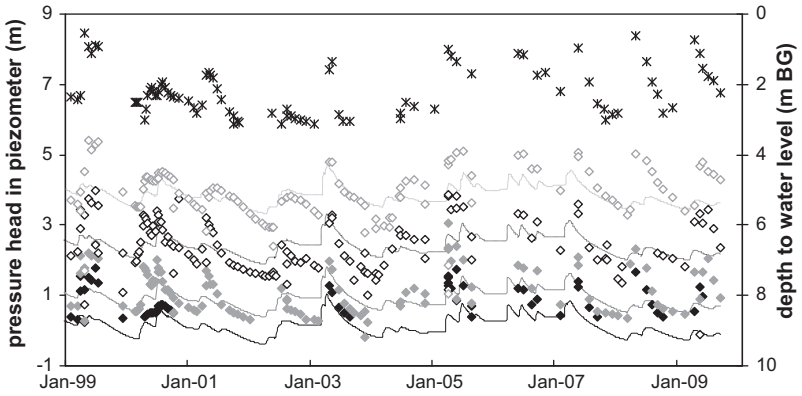

Fig. 2. Measured (symbols, left y-axis) and simulated pressure heads (lines, left y-axis) in shallow piezometers (2.0 m, solid black; 3.0 m, solid gray; 4.5 m, open black, 6.0 m, open gray) as well as water levels measured in the water table well (stars, right y-axis).

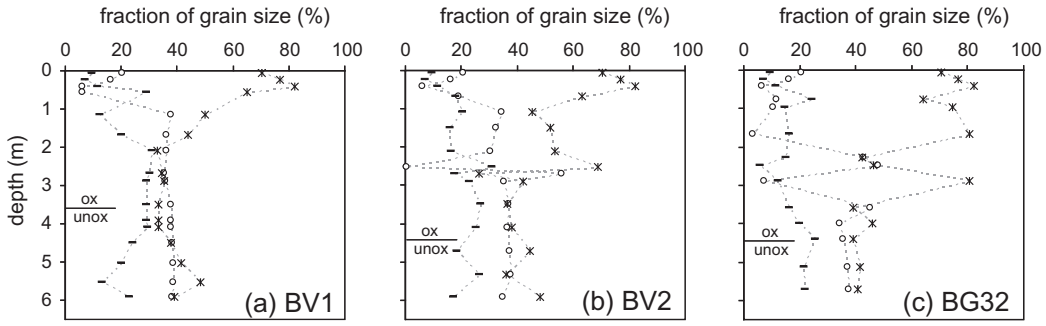

Fig. 3. Sand (circles), silt (stars), and clay (dash) fractions vs. depth at (a) BV1, (b) BV2, and (c) BG32. The transition from the oxidized to unoxidized till is at 3.6 m for BV1 and at 4.4 m for BV2 and BG32.

to the upper 2 m (2.5Y 6/1, dry; 2.5Y 6/2, dry), respectively. The transition from the oxidized to unoxidized zone was identified by an abrupt change to darker colors at 3.6 m BG at BV1 (2.5Y 5/1, dry) and at 4.4 m BG at BV2 (10YR 5/1, dry) and BG32 (2.5Y 5/1, dry). The boundary is not associated with a change in particle-size distribution or with the depth of the present-day water table level in the water-table well.

Differences among the three sites are also evident in the bulk density (data not presented), volumetric water content, and porosity data (Fig. 4). Mean values and standard deviations were calculated per depth for each site for the three sampling campaigns in 2009. Relatively high standard deviations of the porosities and bulk densities particularly reflect the spatial heterogeneity of the sediments and also the difficulty in collecting representative volumetric sub-samples (e.g., without deformation of the soil core). Although the cores were mostly intact, swelling and/or compaction of the cores occurred during sampling and could have resulted in the small observed differences between porosities and water contents, particularly below the measured water table (>2.25 m BG) where these values should be equal. Little changes in volume due to the sampling procedure would have a great impact on water content and porosity measurements. For example, if the diameter and the length of the 0.1 m subsamples increase only by 0.002 m (=2%) and assuming a saturated water content of 0.40, would result in a difference of 0.03 between measured porosity (0.43) and water content (0.40).

In general, porosity values decrease and bulk densities increase with depth at all three sites. However, porosities at BV2 and BG32 attain maximum values at 2.5 m and 2.8 m BG, respectively, reflecting a change in texture (a decrease in sand and increase in silt fractions) (Figs. 3b, c and 4b, c). Volumetric water contents are consistent with gravimetric water content data (data not presented). The water content varies at all three sites above the maximum depth of water table (<2.25 m BG) measured in the WTW during the sampling campaigns suggesting variable saturated conditions. However, greater differences between the volumetric water content and porosity at BV1 (up to a difference of 0.2 $m^3 m^{-3}$) suggest unsaturated conditions between 1.5 and 2.5 m BG during the entire observation period (Fig. 4a). This observation is not consistent with measurements from the WTW, which suggest that the water table decreases from 1.1 m to 2.25 m BG. If the water table depth was constant across the site, the sediments should have been permanently saturated below 2.25 m BG and at 1.1 and 1.8 m BG during the first and second sampling campaigns. This is not the case at BV1. Therefore, either the depths to the water table were not uniform across the site or the measured water content and porosity values are erroneous. We excluded the latter possibility because differences attributed to the sampling procedure would be smaller as indicated above, and, even more important, similar porosities were obtained for the analysis of the water retention functions (Fig. 5); generally, similar water retention characteristics are observed throughout the entire BV1 profile (Fig. 5). The measured water contents were generally parallel with increasing pressure heads for all measured depths. Fitting measured water contents to a unimodal van Genuchten model with SHYPFIT 2.0 (Peters and Durner, 2006) yielded similar parameters for samples from all three soil horizons and the till (Table 1) resulting from almost parallel water retention functions. The residual water content was not measured and was set at 0.26 above 1 m BG and at 0.20 below 1 m BG due to the shape of the suction points; however, this was less important as the suctions in the zone of the water table fluctuations were smaller and did not approach such dry conditions. These functions support the measured water contents and the presence of a deeper water table at BV1

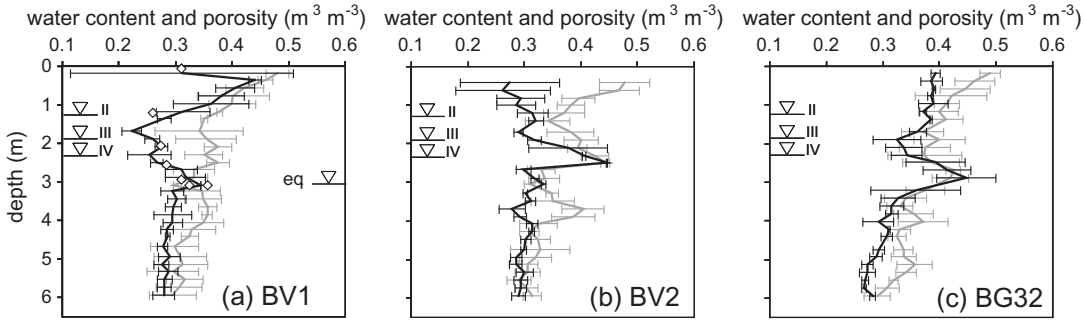

Fig. 4. Porosities (gray) and volumetric water contents (black) vs. depth at (a) BV1, (b) BV2, and (c) BG32. Mean values and standard deviation were calculated from three sampling campaigns. The depths to the water table measured at the water-table well are provided for each sampling campaign (II–IV; inverted triangles). Theoretical water contents calculated from measured water retention characteristics are given for BV1 (symbols) assuming a water table at 3.1 m BG and equilibrium conditions (no flow, capillary rise).

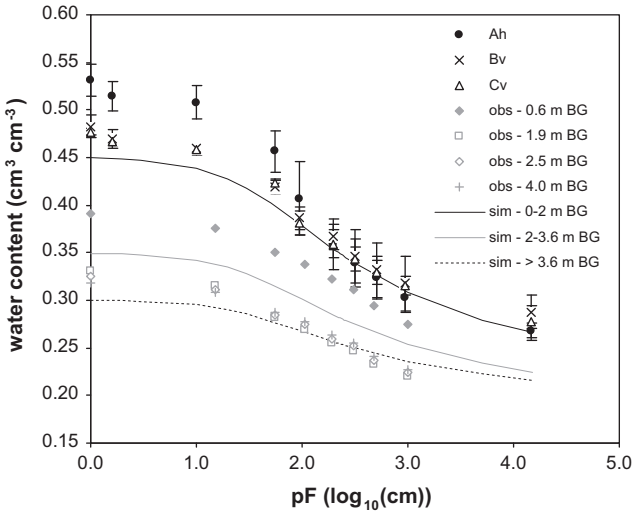

Fig. 5. Measured (symbols) water retention characteristics of the three soil horizons (Ah, Bv, Cv) and at four different depths of the BV1 core samples as well as water retention characteristics obtained from the model simulations for three different depth layers.

Table 1
Hydraulic parameters measured in drainage experiments and *in situ* using a Guelph permeameter and used for equilibrium modelling.

	Depth (m)	θ_s ($m^3\,m^{-3}$)	θ_r ($m^3\,m^{-3}$)	α (m^{-1})	n	K_s ($m\,s^{-1}$)
Measured						
soil	0.04	0.52	0.26	2.5	1.54	–
	0.19	0.48	0.27	3.9	1.40	10^{-6}–10^{-8}
	0.37	0.48	0.26	3.4	1.37	10^{-6}–10^{-8}
till						
BV1	0.57	0.40	0.26	3.4	1.48	
	1.90	0.33	0.20	3.8	1.41	
	2.50	0.34	0.20	4.7	1.46	
	4.02	0.33	0.20	3.8	1.41	
BV2	0.57	0.40	0.26	4.7	1.58	
	1.70	0.34	0.20	8.8	1.20	
	2.60	0.33	0.20	5.2	1.19	
	3.92	0.38	0.20	5.1	1.24	
BG32	0.57	0.45	0.26	6.7	1.14	
	1.70	0.39	0.20	2.0	1.23	
	2.50	0.40	0.20	0.9	1.12	
	3.82	0.34	0.20	3.1	1.18	
Modelling						
BV1	0–2.0	0.45	0.23	3.4	1.30	5×10^{-6}
	2.0–3.6	0.35	0.20	3.4	1.30	10^{-8}
	3.6–6.0	0.30	0.20	3.4	1.30	10^{-10}
BV2	0–2.0	0.40	0.17	3.4	1.30	5×10^{-6}
	2.0–4.4	0.40	0.23	3.4	1.30	10^{-8}
	4.4–6.0	0.30	0.23	3.4	1.30	10^{-10}
BG32	0–2.0	0.48	0.23	3.4	1.30	10^{-6}
	2.0–4.4	0.43	0.23	3.4	1.30	10^{-8}
	4.4–6.0	0.30	0.23	3.4	1.30	10^{-10}

than at the other two soil profiles. Assuming a water table depth of 3.1 m BG at BV1 and equilibrium conditions (no flow and only capillary rise), the respective water contents from the water retention functions were calculated. The theoretical results agreed with the measured water content distribution and suggest a water table of 3.1 m BG at this site. The differences between 0.5 and 1 m BG, where we measured saturated conditions, can be explained by a layer with a greater clay content (29%) than those above or below it (~12%) (Fig. 3a). This layer could act as a capillary barrier.

Distinct peaks of elevated electrical conductivity (EC) in a depth profile about 10 m from BV1 (data from Harrington and Hendry, 2006) is consistent with the presence of local saturated (perched) conditions above 1.1 m BG (accompanied by 800 mS m^{-1}) and a permanent water table at about 3 m BG (accompanied by 500 mS m^{-1}) (Fig. 6a). Increasing EC up to 0.5 m BG (1400 mS m^{-1}) is also attributed to higher clay content (Fig. 3a) and increased porosity (Fig. 4a) (Schulmeister et al., 2003). Minor differences between volumetric water contents and porosities (<0.06 m^3/m^3) at BV2 suggest unsaturated conditions between 1.5 and 2.0 m BG. EC measurements near this site (3 m away, data from Harrington and Hendry, 2006) is generally low (<100 mS m^{-1}) near the surface (<1 m), indicating no salt and dry conditions (Fig. 6b). A slight peak in EC (200–300 mS m^{-1}) measured between 1.9 and 2.5 m BG provides evidence for a potential water table at ~2.2 m BG in September 2009 and the observed increase in porosity at 2.5 m BG (Fig. 4b). An EC step was measured at 3 m BG at BG32 (Fig. 6c, Harrington and Hendry, unpublished data). This is also attributed to increased porosity (Fig. 4c) of a layer with a greater sand content (Fig. 3c). EC remained almost constant (1000 mS m^{-1}) above 2.5 m (Fig. 6c) and suggests a water table at this depth and high water contents above, consistent with observations from the site (Fig. 4c).

3.3. Water isotopes

Monthly water isotope values in precipitation from Saskatoon (Environment Canada, unpublished data) were collected between 1990 and 2009. The mean monthly distribution for this time period is shown in Fig. 7. These data were used to develop a Local Meteoric Water Line (LMWL) of $\delta^2H = 7.7 \cdot \delta^{18}O - 3.1$ (Fig. 8) for the site. Mean weighed (unweighed) annual values for δ^2H and $\delta^{18}O$ in precipitation are −112‰ (−131‰) and −14.6‰ (−16.8‰), respectively. Mean weighed (unweighed) summer values are −98‰ (−106‰) for δ^2H and −12.5‰ (−13.6‰) for $\delta^{18}O$; weighed (unweighed) winter values are −160‰ (−163‰) for δ^2H and −20.0‰ (−20.9‰) for $\delta^{18}O$.

Mean isotope composition and standard deviations were calculated for every depth (Fig. 8) for each site to compare gross trends in the dynamics of water isotopes in the upper 6 m. Regression lines for mean isotope compositions differ in slope and intercept. Slopes less than that of the LMWL indicate isotope values enriched due to sublimation and/or evaporation effects. This effect is most pronounced in samples from BG32 and least pronounced in those from BV1. The regression lines generated for BV1 and BV2 have similar slopes and intercepts. Statistical analyses comparing mean values of the isotope compositions among the three sites indicate BV1 (−146‰) and BV2 (−149‰) are not different (unpaired *T*-test, $p > 0.05$), whereas both differ from BG32 (−141%) (unpaired *T*-test, $p < 0.05$). With respect to variances, BV1 is different from both BV2 and BG32 (*F*-test, $p < 0.05$), but BV2 and BG32 are not different (*F*-test, $p > 0.05$). These statistics suggest processes at BV1 and BV2 may be similar (same mean isotope compositions), with both differing from BG32.

In general, mean isotope values in pore water are depleted compared to the annual weighed precipitation (−112‰), suggesting a greater relative contribution of winter precipitation and snowmelt to the recharge. This is supported by (i) the actual mean isotope values in precipitation ranging from −191‰ to −128‰ during winter (Fig. 7) and (ii) observations from the water table well, whereby the water table increased due to snowmelt in spring and then slowly decreased over the rest of the year. Data from BV1 (Fig. 8a) exhibit the greatest range in δ^2H values (−107‰ to −157‰) when compared to the other two sites, where values ranged from −124‰ to −158‰ (BV2; Fig. 8b) and −125‰ to −149‰ (BG32; Fig. 8c). The isotopic data clustered into discrete depth regions for each site. The values with the greatest standard deviation (Fig. 8; error bars) are typically encountered near the soil surface. Three regions can be identified at BV1 (Fig. 8a): the most enriched

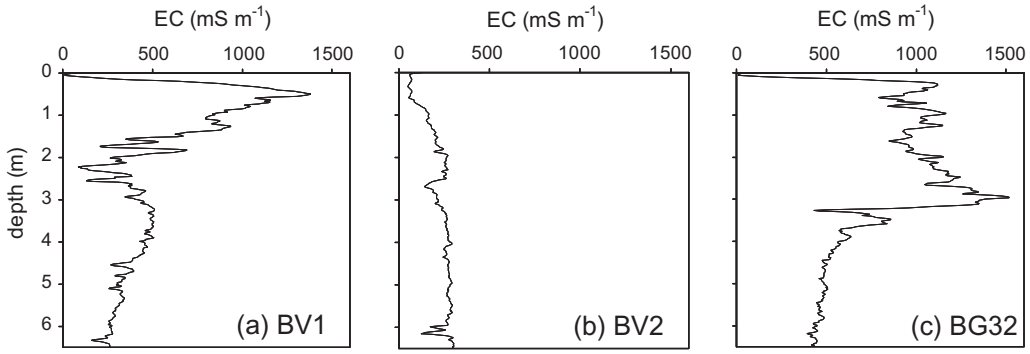

Fig. 6. Electric conductivity measurements (EC) vs. depth close to (a) BV1, (b) BV2, (both according to Harrington and Hendry, 2006) and (c) BG32 (Harrington and Hendry, unpublished data).

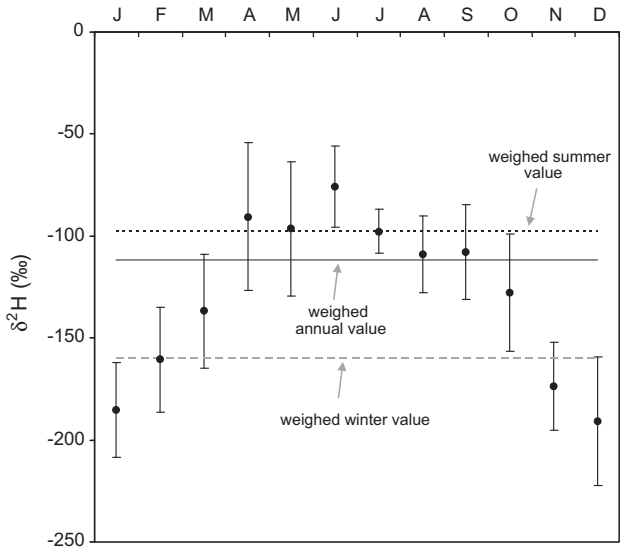

Fig. 7. Mean weighed monthly values (symbols) of δ^2H in Saskatoon precipitation (1990–2009); mean weighed annual (black solid line), summer (black dashed line), and winter (gray dashed line) value.

isotope values (>−133‰ δ^2H) near surface (<0.7 m BG); depleted values (−137‰ to −155‰ δ^2H) between 0.8 and 2.1 m BG and below 3 m BG; and even more depleted values (<−155‰ δ^2H) between 2.2 and 3 m BG. Three depth related zones can also be identified at BV2: the most enriched values (−124‰ δ^2H) above 0.3 m BG; the most depleted at 0.5–0.7 m BG (−158‰ δ^2H); and intermediate values below 0.8 m BG (Fig. 8b). Unlike BV1 and BV2, isotope values at BG32 generally decrease from near ground surface (−125‰) to the base of the site (−147‰); values near the surface (<0.5 m BG) are more enriched (>−131‰ δ^2H) (Fig. 8c).

At all sites, the enriched values near ground surface and the smaller slope of the regression line compared to the LMWL suggest the pore water is affected by sublimation and/or evaporation. If evaporation and sublimation only occurs at the soil surface, similar distributions of mean isotope values and slopes of the dual isotope plot would be expected at all three sites. As this is not the case, isotope evaporation effects in the subsurface and different evaporation rates at the individual sites may have altered the isotope signatures as is shown for arid regions (Barnes and Allison, 1988). Greater relative slopes of pore water regression lines (e.g., BV1, BV2) are generally attributed to sublimation effects and smaller relative slopes (e.g., BG32) to evaporation (Clark and Fritz, 1997). The influence of evaporation is supported by spatial EC distributions at the King Site (Harrington and Hendry, 2005, 2006). Water flows upwards and evaporates while salts accumulate in the unsaturated zone above the water table, which results in the greatest total EC in the upper 2 m near BG32 (about 1700 mS m^{-1}, see Fig. 6c), moderate levels near BV1 (about 1000 mS m^{-1}), and lower values near BV2 (about 300 mS m^{-1}, see Fig. 6a) (Harrington and Hendry, 2005, 2006).

All three sites differed with respect to isotope distribution with depth, but approached similar values at 6 m (−149.8 ± 2.6‰) (Fig. 9). Below this depth, the δ^2H continues to decrease and

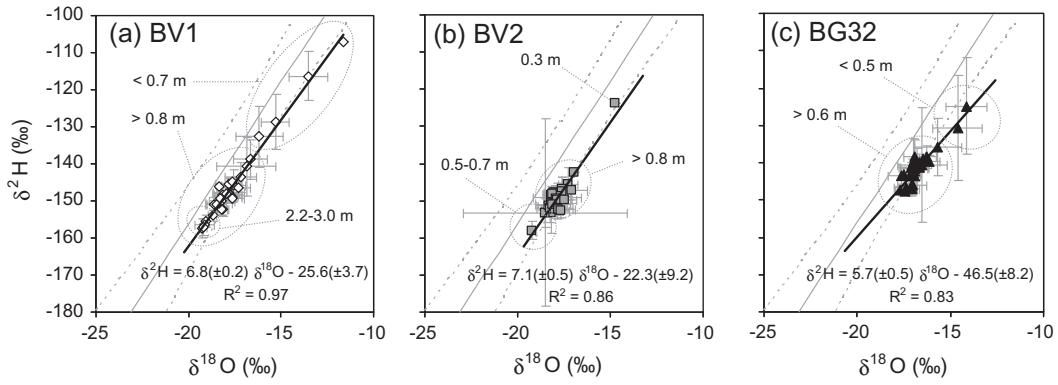

Fig. 8. LMWL (gray, solid) and 95% confidence intervals (gray, dashed) of Saskatoon precipitation (1990–2009) and measured mean isotope composition of pore waters (symbols) and their regression lines (black, solid) at (a) BV1, (b) BV2, and (c) BG32. Mean values and standard deviations were calculated per depth from three sampling campaigns.

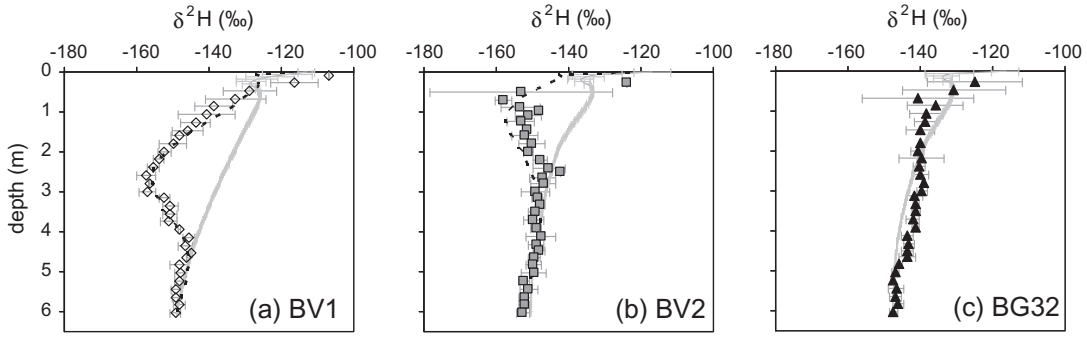

Fig. 9. Measured mean δ^2H (symbols) vs. depth and simulated depth distributions (lines) at (a) BV1, (b) BV2, and (c) BG32. Mean values and standard deviations were calculated from three sampling campaigns with different water table depths BG.

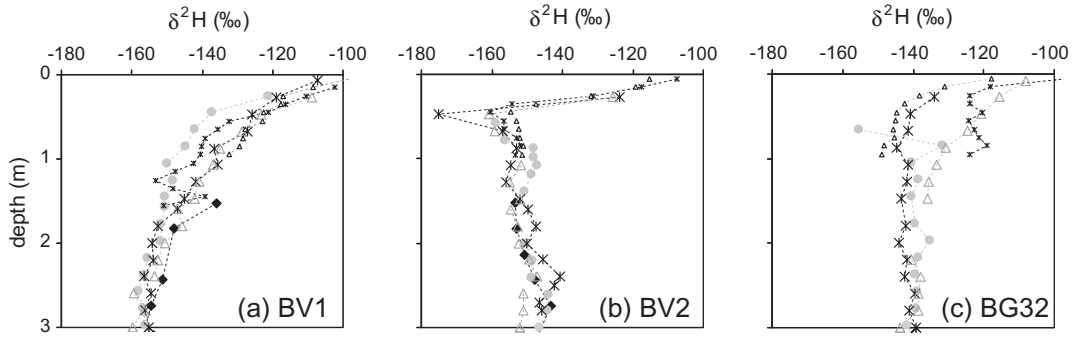

Fig. 10. Temporal development of δ^2H in the upper 3 m measured in core samples (large symbols) and hand auger samples (small symbol) at (a) BV1, (b) BV2, and (c) BG32 from four sampling campaigns (I-December 2007, black diamonds; II-June 2009, gray circles; III-July 2009, black stars; and September IV-2009, gray triangles).

approach similar values for BV1 and BV2 at depths >14 m (<−166‰) (Hendry and Wassenaar, 2009). The isotope values at BV1 decrease continuously to 3 m BG and then increased to 4.5 m BG, below which they remain relatively constant (Fig. 9a). Variations between the sampling campaigns greater than two times the measurement accuracy (±4‰) are apparent to depths of 1.5 m. Isotope values were more depleted in spring and became more enriched throughout the remainder of the year (Fig. 10a) suggesting a degree of mixing of pre-event (more negative winter isotope values) and event water (less negative summer isotope values). Below 1.5 m, no significant temporal change in the isotope values was measured during the year. At BV2, local δ^2H minima and maxima are observed at 1 m and 2.5 m BG. At depths >2.5 m, δ^2H slowly decreases. Differences in δ^2H (>4‰) between the sampling campaigns are evident to a depth of 2.4 m BG at BV2 (Fig. 10b), reflecting some seasonal isotope variations with depth and suggest minimal recharge from precipitation events throughout the year (which get mixed with pre-event soil water).

No isotopically-depleted zone occurred at BG32 during the observation period (Fig. 9c). Depleted winter isotope contents (−158‰) are only evident at 0.6 m depth in June 2009 (Fig. 10c). This value is subsequently attenuated (July 2009) and finally enriched (September 2009) at the end of the observation period. Generally, a continuous depletion of water isotopes with depth was observed below 1.1 m for all observation periods (standard deviations <4‰) at BG32. This δ^2H depth distribution shows the most enriched values (mean value) and the greatest variability near the surface. This variability is attributed to spatial heterogeneities and is accentuated by differences between the δ^2H of the hand auger profiles and the cored profiles collected during the July and September sampling campaigns (Fig. 10c). In both cases, differences in δ^2H of about 40‰ are apparent over a lateral distance of only 2–3 m. Such spatial heterogeneities could result from the presence of zones of slow movement water juxtaposed with areas of enhanced movement or finger flow (Nieber, 1996; Rosenbom et al., 2009; Vogel et al., 2000; Wang et al., 2004). The presence of heterogeneous fracture distributions is supported by EC measurements and salt crystal occurrence (secondary gypsum). Salt accumulations along preferential flow paths (crystals) and in the matrix (crust) were clearly visible above 2.5 m in wet and dry core samples from BG32, respectively; below 2.5 m, no crystals were evident. Crystals along fractures were non-uniformly distributed within cores and with depth. In addition, more crystals were observed in cores from June 2009 than in cores from September 2009. Consequently, fracture density, spacing, and direction appear strongly heterogeneous above 2.5 m at BG32, both in the vertical and horizontal direction. This results in large differences in EC (±400 mS m^{-1}) over a short distance (<10 m) (Harrington and Hendry, 2006) and in greater variability of isotope values in the cores from June and September 2009 near the surface within 3 m lateral distance (Fig. 10c). These observations suggest the density and connectivity of fractures are locally strongly heterogeneous at BG32 and that the greater K_s in fractures connected to the surface result in greater evaporative loss. As near saturation conditions (Fig. 4c) and high EC were measured (Fig. 6c), evaporative loss is suggested to be accompanied by a steady supply of water due to capillary rise and upward fluxes. Therefore, more enriched mean isotope values (−141‰) were measured compared to the other sites, where lower EC was measured and only some (BV1) or even minor (BV2) salt crystals were noticed in the core samples.

Salt accumulations along fractures in cores were observed and had irregular patterns in the upper 3 m BG at BV1. Evidence of salt crystals decreased with depth and no precipitated salts were visible below 3 m BG. Thus, the local minimum in EC (250 mS m^{-1}) at about 2 m BG (Fig. 6a) can be attributed to low water contents as discussed above, rather than absence of salts. As crystals along

fractures were evident in the clay rich layer and in the underlying unsaturated zone, the flow systems at BV1 appear continuously connected to the water table and net upward fluxes are likely, although to a lesser extent than at BG32. This is also confirmed by the shape of the isotope profiles above and below the minimum at 3 m BG. If transport was dominated by diffusion only, this shape would be asymmetrical due to lower effective diffusion coefficients in the unsaturated zone. However, the shape is more symmetrical and the reduced effective diffusion in the unsaturated zone may be offset by upward fluxes with more depleted water isotope values, resulting in the measured water isotope distribution above and below 3 m BG.

Individual salt crystals were evident at 2.1, 3, and 4.3 m BG at BV2. However, no crystals were evident along fractures in wet samples and no visible salt crusts were noted on surfaces of dry samples. These findings are corroborated by low EC values (Fig. 6b). Therefore, evapotranspiration appears restricted to the upper 0.3–0.5 m due to relatively small hydraulic conductivities in the nonfractured matrix at BV2.

3.4. Modelling

The upper boundary for the modelling was assigned atmospheric conditions for water flow and concentration fluxes for δ^2H. Daily input parameters (precipitation, ETp, and water isotopes of precipitation) for the past 10 years were run ten times to yield a simulation period of 100 years to allow changes resulting from the low flow velocities to be observed. Only evaporation was accounted for in the model because the prairie grass vegetation across the site was sparse and the visual depth of rooting in the core samples was observed to be shallow; the root density decreased considerably between 0.1 and 0.3 m BG over the site and no roots were observed below 0.3 m BG. Further, root growth or root water uptake parameters in the model were not known. Isotopic enrichment was not included in the model. This assumption was considered to have a minor impact on the simulations because although the slopes of the regression lines were different, they remained similar to the LWML, suggesting limited effects of enrichment (Fig. 8).

The lower boundary was located at 6 m BG and assigned a zero water flux. This assumption was considered appropriate because the water velocity through the unoxidized till is very small. The mean measured isotope content at 6 m BG at each corehole was used to define a lower concentration boundary. Initial conditions were generated by establishing a water table at 2 m BG and assigning constant isotope concentrations equal to the lower boundary concentration. Hydraulic parameters (Table 1) for the soil and the till were averaged for each profile and were assigned according to the texture, soil color (oxidized/unoxidized zone), and measured porosities. Thus, three horizons with different porosities were assumed. Measured K_s values near ground surface were used to provide an initial order of magnitude and inversely improved to obtain a best fit. Moreover, α and n were also inversely improved. Dispersivities were set constant for all sites and throughout depths (α_L = 0.01 m). The δ^2H diffusion coefficient (10^{-9} m^2 s^{-1}) was calculated according to Mills (1973).

The simulated mean distribution of δ^2H for the dates of the three sampling campaigns were compared against the measured values after the 100-year simulation period because the differences in depth distribution between the sampling campaigns as well as the simulations was small. The resulting, simulated δ^2H-profiles were similar for all three soil profiles (Fig. 9, solid line), largely due to the similarities in measured and fitted water retention characteristics. All results indicate diffusion controlled solute transport both below the water table and shallower (>0.7 m BG). At depths <0.7 m, water fluxes appear to impact transport processes, resulting in a seasonal isotope trend.

The simulated pressure heads within the profiles demonstrate similar trends to the measured pressure heads in the shallow piezometers (Fig. 2). The model was most accurate for BG32 (Fig. 9c, solid line), where the simulated δ^2H profile is in the range of the spatial variability. Equilibrium solute transport seems generally capable of reproducing measured isotope values for this site.

Adequately simulating the more depleted measured isotope profiles at BV1 and BV2 was not possible, suggesting isotope transport processes at these sites are more complex than can be described by this simple 1-D model. Two causes for this complexity were considered: preferential vertical flow and lateral flow. The effects of preferential, vertical downward flow on the profile (i.e., above the water table and near to the soil surface) at BV2 were investigated using a mobile–immobile transport model. Although changing the ratio of mobile and immobile water resulted in greater seasonal differences, mean values calculated according to the three sampling campaigns remained similar to the equilibrium simulations (data not presented), suggesting preferential, vertical flow cannot generate the measured depleted values.

Preferential, lateral flow of depleted winter isotope values originating from infiltration of snowmelt water could result in differential isotopic profiles at BV1 and at BV2. Lateral flow through high permeable, coarser textured sediments within glacial tills can result from depression-focused recharge in landscapes with undulating topography (Gerke et al., 2010). At other sites across glaciated prairies in Canada, lateral flow infiltrates from ephemeral wetland ponds and depressions collecting snowmelt water (Hayashi et al., 2003; van der Kamp and Hayashi, 2009). While the pore water closer to the surface is frozen, thawing in the surrounding of lakes is increased by trapped radiation and thus energy in the water filled depressions resulting in lateral infiltration patterns of partially frozen soils (Hayashi et al., 2003). Similar processes may have occurred at the King Site, where lateral flow mainly infiltrates from the man-made ditch, which was constructed within the last 100 years across the northern portion of the research site (Harrington and Hendry, 2005). Assuming a mean horizontal K_s of 10^{-6} m s^{-1} (which might be greater in fractures or permeable layers), a mean hydraulic gradient of 1 m × 50 m^{-1} (BV1), and a mean porosity of 0.35 would result in flow velocities of 1.8 m a^{-1}. Thus, on average, it would require about 30 years for snowmelt derived water to reach BV1. This time period would decease dramatically if the permeable layers had an estimated K_s of 10^{-2} m s^{-1} (Harrington et al., 2007) or if lateral flow was controlled by low porosity fractures.

3.5. Conceptual model of water migration in a heterogeneous surficial till

A conceptual model is presented that is consistent with the measured data. It is based on the conceptual model proposed by Hayashi et al. (2003) but provides additional insight into spatial and temporal dynamics of lateral and vertical water flow and transport in heterogeneous glacial tills (Fig. 11). This model may be applicable to other sites containing clay-rich sediments with low infiltration capacities and depression focused recharge.

In winter, the water table is at its greatest depth BG and snow accumulates on the frozen ground. In spring, the snowmelt flows laterally to the surface drain on ground surface because the soil is frozen and it cannot infiltrate into the soil. The snowmelt runoff, which is depleted in both isotopes of water, collects in the ditch, where it slowly infiltrates into the unfrozen and/or thawed ground causing the water table to rise. With time, this mound propagates away from the ditch in more permeable zones in the oxidized till. In general, the elevation of the water table decreases with increasing distance from the ditch and time. Mounding beneath the ditch transports the winter isotope signal (in the runoff) laterally and to

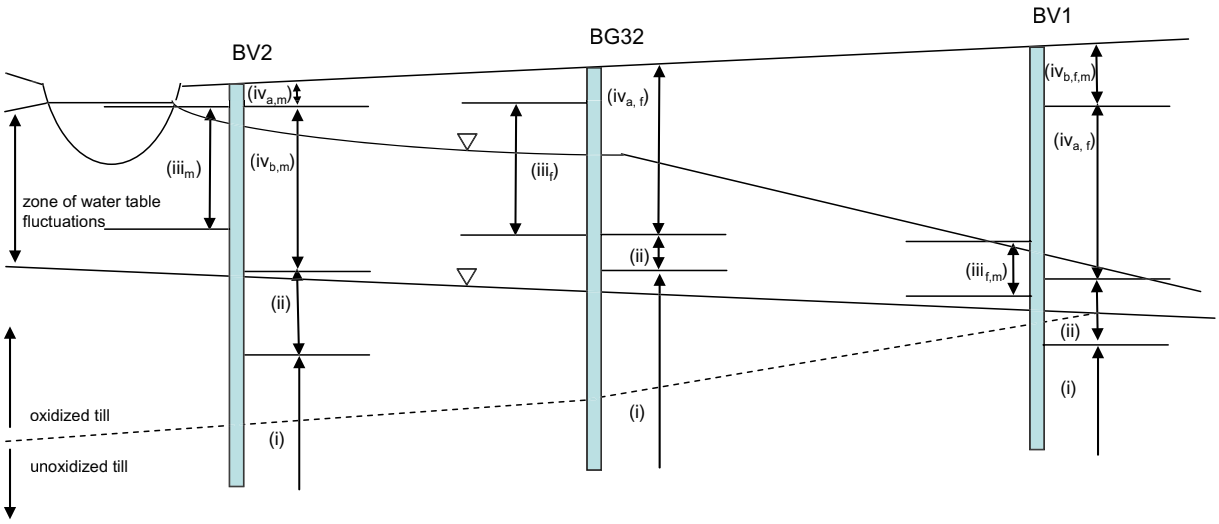

Fig. 11. Hypothetical depth zones and processes across the site. Processes are not related to the zone of water table fluctuations or the oxidized/unoxidized till boundary; (i) long-term stagnant flow and diffusion controlled "historic" transport, (ii) stagnant flow and diffusion controlled mixing between historic and recently influenced zones, (iii) recently induced lateral dominated flow and advective transport in fractures (*f*) and/or transport in the matrix (*m*), and (iv) current upward (*a*) and downward (*b*) fluxes in fractured (*f*) and/or unfractured (*m*) oxidized till.

greater depth with distance from the ditch over the remainder of the hydrologic cycle. The vertical range of depleted isotope values and its absolute minimum value are controlled by the initial saturation of the zone above the winter water table and the distance from the ditch. The farther away and/or the closer to saturation, the less the winter signal will be observed because the signal becomes less depleted during transport (dispersion, diffusion with the matrix) and the relative contribution of the winter signal is minor if the volumetric water content is closer to saturation. The distances from BV2, BG32, and BV1 to the ditch are 10, 30, and 50 m, respectively; therefore, the depleted zone is found deeper below ground at BV1 compared to BV2. The mean degrees of saturation in the zone of water table fluctuations are 80%, 89%, and 95% at BV1, BV2, and BG32, respectively. Therefore, the depleted zone is more pronounced at BV1 and BV2 and all but absent at BG32. In addition to lateral flow, vertical movement influences water content and isotope depth distributions, particularly above the water table and during summer. This influence is highly complex being dictated by spatial and vertical structural heterogeneities. Dominant upward or downward water fluxes are observed, and thus isotope evaporation effects are more or less pronounced in regions with greater or lesser fracture densities, respectively. For example, in regions with small surficial K_s (i.e., no fractures or low density of fractures, such as at BV2) evaporation is restricted to the upper few centimeters of the soil. Surficial water contents decrease over time and upward fluxes slow. In this case, the water table slowly declines due to lateral movement. Below this uppermost region, depleted isotope values are maintained and slowly transported downwards, mainly driven by lateral propagation of the water table mound.

In contrast to regions with relatively small surficial K_s indicating a net downward flux, regions with net upward fluxes are associated with relative large K_s (i.e., regions with fractures and particularly with high fracture density and connectivity to greater depths, such as at BG32). Water contents remain near saturation due to continuous relatively high upward fluxes through fractures that are continuous to below the water table depth. Thus, isotope values are enriched due to evaporation effects in the subsurface. Such fractured structures were identified from EC measurements (Harrington and Hendry, 2005, 2006) and supported by visual observations of secondary gypsum crystals along fractures. Here, the contribution of fractured flow and thus the isotope values can vary within short distances. Whether the absence of an obvious depletion zone in highly fractured systems, such as BG32, is overlapped by the evaporation effect or results from bypass flow is not known.

Less obviously dominant upward or downward movement can be attributed to vertically heterogeneous K_s values, due to heterogeneities in particle size distribution and variable fracture density with depth. Local low permeability layers in the unsaturated zone are suggested to remain near saturation even close to the surface (e.g., BV1). Infiltration after heavy rain events, being isotopically enriched, preferentially flows through fractures and partially perches at such layers. However, a net evaporative loss through fractures might penetrate to deeper regions, as suggested by EC measurements and visual observations of crystals at BV1.

In summary, the conceptual model presented in Fig. 11 identifies flow processes associated with different zones. It does, however, remain to be tested. The validation of the conceptual model through development of a mathematical water flow and water isotope transport model is not feasible at the present time because one of the major obstacles in soil physics and hydrogeology is the lack of an adequate description of non-equilibrium flow and transport (Šimůnek et al., 2003). In the present study, the clay-rich sediments are highly heterogeneous, with non-equilibrium flows as the rule rather than the exception. This finding is supported by other research (Flury et al., 1994; Ritsema and Dekker, 2000). At the present site, a 2D model cannot reproduce the measured results. A 3D approach may work, although the required model input data (e.g., soil properties) may not be measureable at sufficient resolution and crucial processes are still unknown or not available in model codes. The latter includes processes such as soil frost and water flow in frozen soils (Okkonen and Klove, 2010). Another obstacle to developing a mathematical water flow and water isotope transport model is the quantification of the transport of water isotopes. Water isotopes are an integrative tracer in time and space, but transport is not simple because the ratio of water isotopes can be affected by fractionation processes (Clark and Fritz, 1997). This is particularly relevant in cases where phase changes, such as sublimation of snow, aging within the snowpack, freezing, and evaporation, play a major role in altering the isotopic ratio. To date, no 2D or 3D, non-equilibrium transport models include water isotope fractionation processes.

4. Summary and conclusions

This study showed that the structure of glacial tills can be highly heterogeneous over short vertical and lateral distances. Thus, water flow and transport processes are highly complex and dynamic and can result in variable chemical, physical, and isotopic distributions. As a result, such sites must be sampled with high spatial (depth and distance) resolution. Measurements of chemical parameters (EC) or sediment parameters (e.g., water contents, hydraulic conductivities, bulk densities) alone may be insufficient to describe heterogeneous water flow patterns and may result in incorrect conclusions being drawn without consideration of all parameters. Similarly, incorrect conclusions can also be drawn from results of 1D flow and transport calculations not reflecting the complex dynamic and heterogeneous processes. Thus, additional investigations, including measurement of water isotopes in conjunction with visual analysis of core samples, can be crucial for identifying water flow and solute transport processes and are thus highly recommended. With respect to the water isotopes, the current study shows that considerable information about dynamic and heterogeneous flow and solute transport can be gained from the water isotopes in pore waters, particularly from high-resolution profiles of stable isotopes that can be easily measured in the unsaturated and saturated zone using laser spectroscopy.

In this study, four main depths zones with different processes were identified. These zones partially overlap each other due to dynamic variability and are not uniform across the site, both with respect to processes and spatial dimensions. In addition, they are not related to the mean water table, the elevation (microtopography), or the transition between the oxidized and unoxidized till. Further, extrapolating water tables or transitions between the oxidized and unoxidized till uniformly across a (small) site as well as assuming homogeneous chemical distributions or uniform fluxes may result in erroneous conclusions about transport processes.

Four flow processes are associated with the four zones: (i) long-term stagnant flow and diffusion controlled "historic" transport, (ii) stagnant flow and diffusion controlled mixing between historic and recently influenced zones, (iii) recently induced lateral dominated flow and advective transport in fractures or/and the matrix, and (iv) current surface near upward and downward fluxes in fractured and unfractured oxidized till. The transition between historic and more recent processes is accompanied by an enriched isotope peak that can be seen as the lower end member for recent transport and as the upper boundary for historic considerations. This peak will diminish with time and propagate deeper below ground. Due to heterogeneities, this peak is not uniform with depth, and the boundary between the oxidized and unoxidized till is neither uniform nor parallel to the surface (neglecting major erosion processes to date). This study demonstrated that ephemeral depressions fed by snowmelt in the spring can induce lateral flow and thus influence the shallow flow system. Similar studies considering pore water isotope depth distributions should be conducted at other fractured till sites close to permanent or ephemeral wetlands and ponds to test this conceptual model.

Acknowledgements

The authors acknowledge Virginia Chostner, Laura Smith, Cody Manchester, Shiva Acharya, and Julie Zettl for assistance with field work and data collection. Glenn Harrington (CSIRO) is gratefully thanked for providing the electric conductivity data. Financial support from the Cameco-NSERC Industrial Research Chair (MJH) is acknowledged.

References

ASTM, 2007. D 422-63: Standard Test Method for Particle-Size Analysis of Soils. In: ASTM International (Editor), Annual Book of Standards West Conshohocken, PA.
Barnes, C.J., Allison, G.B., 1988. Tracing of water movement in the unsaturated zone using stable isotopes of hydrogen and oxygen. J. Hydrol. 100, 143–176.
Blake, G.R., 1965a. Bulk density. In: Black, C.A. (Ed.), Methods of Soil Analysis. American Society of Agronomy, Inc., Madison, Wisconsin, USA, pp. 374–390.
Blake, G.R., 1965b. Particle density. In: Black, C.A. (Ed.), Methods of Soil Analysis. American Society of Agronomy, Inc., Madison, Wisconsin, USA, pp. 371–373.
Christiansen, E.A., 1971. Tills in southern Saskatchewan, Canada. In: Goldthwait, R.P. (Ed.), Till: A Symposium. Ohio State Univ. Press, Columbus, pp. 167–183.
Clark, I.D., Fritz, P., 1997. Environmental isotopes in hydrogeology. Lewis Publishers, Boca Raton, FL.
Cuthbert, M.O., Mackay, R., Tellam, J.H., Thatcher, K.E., 2010. Combining unsaturated and saturated hydraulic observations to understand and estimate groundwater recharge through glacial till. J. Hydrol. 391 (3–4), 263–276.
D'Astous, A.Y., Ruland, W.W., Bruce, J.R.G., Cherry, J.A., Gillham, R.W., 1989. Fracture effects in the shallow groundwater zone in weathered Sarnia–Area clay. Can. Geotech. J. 26 (1), 43–56.
Darling, W.G., Bath, A.H., 1988. A stable isotope study of recharge processes in the English Chalk. J. Hydrol. 101 (1–4), 31.
DePaolo, D.J., Conrad, M.E., Maher, K., Gee, G.W., 2004. Evaporation effects on oxygen and hydrogen isotopes in deep vadose zone pore fluids at Hanford, Washington. Vadose Zone J. 3 (1), 220–232.
Ellis, J.G., Acton, F., Moss, H.C., 1970. The Soils of the Rosetown Map Area, Distributed by the Extension Division, University of Saskatchewan. Modern Press, Distributed by the Extension Division, University of Saskatchewan, Saskatoon.
Flury, M., Flühler, H., Jury, W.A., Leuenberger, J., 1994. Susceptibility of soils to preferential flow of water: a field study. Water Resour. Res. 30, 1945–1954.
Freeze, R.A., Cherry, J.A., 1979. Groundwater. Prentice Hall, Englerwood Cliffs, NJ.
Gardner, W.H., 1965. Water content. In: Black, C.A. (Ed.), Methods of Soil Analysis. American Society of Agronomy, Inc., Madison, Wisconsin, USA, pp. 82–127.
Gerke, H.H., Köhne, M.J., 2004. Dual-permeability modeling of preferential bromide leaching from a tile-drained glacial till agricultural field. J. Hydrol. 289 (1–4), 239.
Gerke, H.H., Koszinski, S., Kalettka, T., Sommer, M., 2010. Structures and hydrologic function of soil landscapes with kettle holes using an integrated hydropedological approach. J. Hydrol. 393 (1–2), 123–132.
Harrar, W., Murdoch, L., Nilsson, B., Klint, K., 2007. Field characterization of vertical bromide transport in a fractured glacial till. Hydrogeol. J. 15 (8), 1473.
Harrington, G.A., Hendry, M.J., 2005. Chemical heterogeneity in diffusion-dominated aquitards. Water Resour. Res. 41, W12432.
Harrington, G.A., Hendry, M.J., 2006. Using direct-push EC logging to delineate heterogeneity in a clay-rich aquitard. Ground Water Monit. R. 26 (1), 92–100.
Harrington, G.A., Hendry, M.J., Robinson, N.I., 2007. Impact of permeable conduits on solute transport in aquitards: mathematical models and their application. Water Resour. Res. 43 (5), W05441.
Hayashi, M., van der Kamp, G., Schmidt, R., 2003. Focused infiltration of snowmelt water in partially frozen soil under small depressions. J. Hydrol. 270 (3–4), 214–229.
Helmke, M.F., Simpkins, W.W., Horton, R., 2005. Simulating conservative tracers in fractured till under realistic timescales. Ground Water 43 (6), 877–889.
Hendry, M.J., Wassenaar, L.I., 1999. Implications of the distribution of δD in pore waters for groundwater flow and the timing of geologic events in a thick aquitard system. Water Resour. Res. 35 (6), 1751–1760.
Hendry, M.J., Wassenaar, L.I., 2009. Inferring heterogeneity in aquitards using high-resolution δD and $\delta^{18}O$ profiles. Ground Water 47 (5), 639–645.
Joergensen, P.R., Fredericia, J., 1992. Migration of nutrients, pesticides and heavy-metals in fractured clayey till. Geotechnique 42 (1), 67–77.
Joergensen, P.R., McKay, L.D., Kistrup, J.P., 2004. Aquifer vulnerability to pesticide migration through till aquitards. Ground Water 42 (6–7), 841–855.
Joshi, B., Maulé, C., 2000. Simple analytical models for interpretation of environmental tracer profiles in the vadose zone. Hydrol. Process. 14 (8), 1503–1521.
Keller, C.K., Van Der Kamp, G., Cherry, J.A., 1988. Hydrogeology of two Saskatchewan tills. I. Fractures, bulk permeability, and spatial variability of downward flow. J. Hydrol. 101 (1–4), 97.
McCombie, C., 1997. Nuclear waste management worldwide. Phys. Today 50 (6), 56–62.
McKay, L.D., Fredericia, J., 1995. Distribution, origin, and hydraulic influence of fractures in a clay-rich glacial deposit. Can. Geotech. J. 32 (6), 957–975.
McKay, L.D., Fredericia, J.M.L., Morthorst, J., Klint, K.E.S., 1999. Spatial variability of contaminant transport in a fractured till, Avedore Denmark. Nord. Hydrol 30 (4-5), 333–360.
Mills, R., 1973. Self-diffusion in normal and heavy water. J. Phys. Chem. 77 (5), 685–688.
Mortensen, A.P., Jensen, K.H., Nilsson, B., Juhler, R.K., 2004. Multiple tracing experiments in unsaturated fractured clayey till. Vadose Zone J. 3 (2), 634–644.
Mualem, Y., 1979. A new model for predicting the hydraulic conductivity of unsaturated porous media. Water Resour. Res. 12, 513–522.
Nieber, J.L., 1996. Modeling finger development and persistence in initially dry porous media. Geoderma 70 (2–4), 207–229.

Okkonen, J., Klove, B., 2010. A conceptual and statistical approach for the analysis of climate impact on ground water table fluctuation patterns in cold conditions. J. Hydrol. 388 (1–2), 1–12.
Peters, A., Durner, W., 2006. Improved estimation of soil water retention characteristics from hydrostatic column experiments. Water Resour. Res. 42 (11), W11401.
Richards, L.A., 1965. Physical condition of water in soil. In: Black, C.A. (Ed.), Methods of Soil Analysis. American Society of Agronomy, Inc., Madison, Wisconsin, USA, pp. 128–152.
Ritsema, C.J., Dekker, L.W., 2000. Preferential flow in water repellent sandy soils: principles and modeling implications. J. Hydrol. 231–232, 308–319.
Rosenbom, A.E. et al., 2008. Fluorescence imaging applied to tracer distributions in variably saturated fractured clayey till. J. Environ. Qual. 37 (2), 448–458.
Rosenbom, A.E. et al., 2009. Numerical analysis of water and solute transport in variably-saturated fractured clayey till. J. Contam. Hydrol. 104 (1–4), 137.
Schulmeister, M.K. et al., 2003. Direct-push electrical conductivity logging for high-resolution hydrostratigraphic characterization. Ground Water Monit. R. 23 (3), 52–62.
Shaw, R.J., Hendry, M.J., 1998. Hydrogeology of a thick clay till and Cretaceous clay sequence, Saskatchewan. Canada. Can. Geotech. J. 35 (6), 1041–1052.
Šimůnek, J., Jarvis, N.J., van Genuchten, M.T., Gärdenäs, A., 2003. Review and comparison of models for describing non-equilibrium and preferential flow and transport in the vadose zone. J. Hydrol. 272 (1–4), 14–35.
Simunek, J., Sejna, M., van Genuchten, M.T., 2005. The HYDRUS-1D Software Package for Simulating the One-dimensional Movement of Water, Heat and Multiple Solutes in Variably-saturated Media. University of Riverside, California.
Singleton, M.J., Sonnenthal, E.L., Conrad, M.E., DePaolo, D.J., Gee, G.W., 2004. Multiphase reactive transport modeling of seasonal infiltration events and stable isotope fractionation in unsaturated zone pore water and vapor at the Hanford Site. Vadose Zone J. 3 (3), 775–785.
Soilmoisture Equipment Corp., 1986. 2800KI Operating Instructions, Guelph Permeameter, Santa Barbara, CA, USA.
Stumpp, C., Maloszewski, P., Stichler, W., Fank, J., 2009a. Environmental isotope ($\delta^{18}O$) and hydrological data to assess water flow in unsaturated soils planted with different crops: case study lysimeter station "Wagna" (Austria). J. Hydrol. 369 (1–2), 198–208.
Stumpp, C., Maloszewski, P., Stichler, W., Maciejewski, S., 2007. Quantification of heterogeneity of the unsaturated zone based on environmental deuterium observed in lysimeter experiments. Hydrol. Sci. J. 52, 748–762.
Stumpp, C., Stichler, W., Kandolf, M., Šimůnek, J., 2012. Effects of land cover and fertilization method on water flow and solute transport in five lysimeters: a long-term study using stable water isotopes. Vadose Zone J. 11. http://dx.doi.org/10.2136/vzj2011.0075.
Stumpp, C., Stichler, W., Maloszewski, P., 2009b. Application of the environmental isotope $\delta^{18}O$ to study water flow in unsaturated soils planted with different crops: case study of a weighable lysimeter from the research field in Neuherberg, Germany. J. Hydrol. 368 (1–4), 68–78.
van der Kamp, G., Hayashi, M., 2009. Groundwater–wetland ecosystem interaction in the semiarid glaciated plains of North America. Hydrogeol. J. 17 (1), 203–214.
van Genuchten, M.T., 1980. A closed-form equation for predicting the hydraulic conductivity of unsaturated soils. Soil Sci. Soc. Am. J. 44, 892–898.
Vogel, T., Gerke, H.H., Zhang, R., Van Genuchten, M.T., 2000. Modeling flow and transport in a two-dimensional dual-permeability system with spatially variable hydraulic properties. J. Hydrol. 238 (1–2), 78.
Vomocil, J.A., 1965. Porosity. In: Black, C.A. (Ed.), Methods of Soil Analysis. American Society of Agronomy, Inc., Madison, Wisconsin, USA, pp. 299–314.
Wang, Z., Jury, W.A., Tuli, A., Kim, D.-J., 2004. Unstable flow during redistribution: controlling factors and practical implications. Vadose Zone J. 3 (2), 549–559.
Wassenaar, L.I., Hendry, M.J., Chostner, V.L., Lis, G.P., 2008. High resolution pore water δ^2H and $\delta^{18}O$ measurements by $H_2O_{(liquid)}$–$H_2O_{(vapor)}$ equilibration laser spectroscopy. Environ. Sci. Technol. 42 (24), 9262.